Salt Delineation From Electromagnetic Data Using Convolutional Neural Networks

Seokmin Oh, Kyubo Noh, Daeung Yoon, Soon Jee Seol, and Joongmoo Byun

***Abstract*— With recent advances in machine learning, convolutional neural networks (CNNs) have been successfully applied in many fields, and several attempts have been made in the field of geophysics. In this letter, we investigated the mapping of subsurface electrical resistivity distributions from electromagnetic (EM) data with CNNs. To begin imaging electrical resistivity using CNNs, we carried out precise delineation of a subsurface salt structure, which is indispensable for identification of offshore hydrocarbon reservoirs, using towed streamer EM data. For training the CNN model, an electrical resistivity model, including a salt body, and corresponding EM data calculated through numerical modeling were used as the label and input, respectively. The optimal weights and biases of the CNN were obtained minimizing the mean-square error between the predicted resistivity distribution and the target label. The final CNN model was selected using a validation data set during training. After training, we applied the trained CNN to test data sets of noisy data and simulated-SEAM data, which were not provided to the network during training. The test results demonstrate that our trained CNN model is stable, reliable, and efficient, and indicate the possibility of successful application of our CNN model to field data. Our study has shown the promising potential of CNNs for identifying defined subsurface electrical resistivity structures that are difficult to find using conventional EM inversion.**

***Index Terms*— Convolutional neural networks (CNNs), electrical resistivity inversion, electromagnetic (EM), salt body.**

I. Introduction

ONE of the greatest problems for accurate identification of hydrocarbon reservoirs in marine environments in geophysical surveys is clear delineation of the salt structure, as reservoirs usually exist beside or beneath salt bodies. To solve this problem, seismic imaging, which can reveal the structural characteristics of subsurface media, has been usually employed [1], [2]. However, due to uncertainty in the velocity model used in seismic imaging and dispersion, and concentration of seismic signals due to the large velocity difference, imaging the sides and bottom of the salt body is particularly challenging. Therefore, many studies have been conducted to attain clearer delineation of subsurface salt structures through additional processing [3], [4] or calculation of seismic attributes [5], [6], going one step beyond conventional seismic imaging. Although these methods have improved salt characterization, human observation is still needed to interpret salt structures in many image sections.

Machine learning (ML) offers advantages in producing complex representations from data and has a very low inference cost once the ML model has been trained. Due to these advantages, various ML approaches have been attempted in the field of geophysics [7]–[9]. Recently, ML has been actively applied to identification of salt bodies using codebook-based learning [10] and convolutional neural networks (CNNs) [11]–[13]. However, because most of these approaches train the model with processed images extracted from seismic data, they encounter problems based on uncertainty in the data used during the processing stage. To mitigate these problems, Wang *et al.* [14] proposed a new method for estimating the shape and position of salt bodies directly from prestacked seismic data. They replaced the problem of identifying salt with a segmentation problem based on UNet architecture [15] and transformed the data from multishot gathers in the *x*-*t* domain into a salt structure in the *x*-*z* domain.

Electromagnetic (EM) methods can identify the electrical resistivity distribution of the subsurface medium and are sensitive to the high-resistance zones associated with salt bodies and nearby hydrocarbon reservoirs. Marine EM methods have widely been applied and have received noteworthy commercial interest [16]. In this letter, we identify salt structures directly from EM data, excluding steps that might lead to erroneous results, similar to the method used by Wang *et al.* [14]. For this purpose, we apply CNN to frequency-domain EM data obtained with a towed streamer EM system, which has the ability to rapidly investigate large areas [17], [18] and has been applied to imaging of hydrocarbon reservoirs using traditional EM inversion techniques [19]–[21]. To generate the input image, the electric field is calculated through numerical EM modeling and arranged on two axes, common midpoint (CMP) and offset, and then adjusted to fit the input size of our CNN structure. The electrical resistivity model, which includes a salt body with arbitrary shape and size, becomes the label. During training, parameters are determined to fit the prediction to the true electrical resistivity value of the subsurface medium, while minimizing the regression loss function and the electrical resistivity model for the input image is predicted. To evaluate the accuracy of salt identification, the predicted electrical resistivity model is segmented into salt and nonsalt, with the threshold of electrical resistivity determined during the training phase. While training, the best-trained model is selected based on the validation error. Finally, the application

Manuscript received August 21, 2018; revised September 19, 2018; accepted October 16, 2018. This work was supported by the Korea Institute of Energy Technology Evaluation and Planning funded by the Korea Government (MOTIE) under Grant 20164010201120 and Grant 20174010201170. *(Corresponding author: Daeung Yoon.)*

The authors are with RISE (Reservoir Imaging With Seismic & EM Technology) Laboratory, Hanyang University, Seoul, South Korea (e-mail: osm79@hanyang.ac.kr; kyubonoh@gmail.com; duyoon@gmail.com; ssjdoolly@hanyang.ac.kr; jbyun@hanyang.ac.kr).

Color versions of one or more of the figures in this letter are available online at http://ieeexplore.ieee.org.

Digital Object Identifier 10.1109/LGRS.2018.2877155

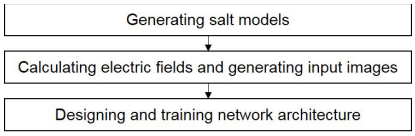

Fig. 1. Overall workflow of this letter.

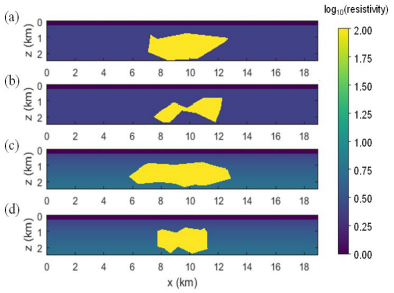

Fig. 2. Resistivity models that contain a salt body embedded in (a) and (b) homogeneous medium and (c) and (d) medium with gradually increasing resistivity.

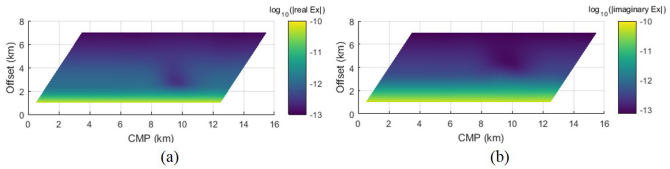

Fig. 3. (a) Real and (b) imaginary data for inline electric fields at 0.4 Hz, shown as CMP plots.

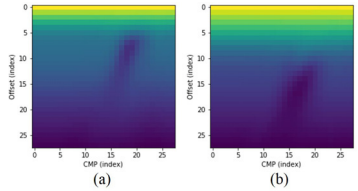

Fig. 4. Examples of input images for the CNN. (a) Real and (b) imaginary data for inline electric fields at 0.4 Hz.

to a more realistic salt model is carried out to validate the architecture. To our knowledge, this is the first attempt to apply CNNs to EM imaging of electrical resistivity structures.

II. Methodology

The overall workflow for delineating salt using towed streamer EM data is shown in Fig. 1. First, we generate electrical resistivity models for a salt body. Next, the electric fields for these resistivity models are calculated using numerical EM forward modeling and resized to match the input images of our CNN. Last, the CNN is designed and trained to estimate the subsurface electrical resistivity.

A. Generating Salt Models

The salt model used for training our CNN consists of two parts: salt body and background. The salt body is constructed by changing the geometrical complexity to create various arbitrary shapes and sizes. The background consists of a 300-m seawater layer with resistivity of 0.33 Ωm and bottom sediments. For the bottom sediments, we consider two different cases: 1 Ωm homogeneous half-space and gradually increasing medium from 1 to 3 Ωm with depth. Based on the salt model conditions, we generated 15 200 different salt models, and randomly split the models into a training set (90%) and a validation set (10%). Those salt models were used for the labels of CNN. Examples of resistivity models including salt embedded in each medium are shown in Fig. 2. The salt models were generated based on a code developed by Kadu *et al.* [22], and the code is available at https://github.com/ajinkyakadu125/ParametricLevelSet.

B. Calculating Electric Fields and Generating Input Images

In the towed streamer EM system, an electric bipole source is towed at a depth of 10 m below the sea surface, and a streamer of electric field receivers up to 9 km long is towed at a depth of approximately 100 m [23]. For this letter, we used the same depth for the source and receivers, with a long EM streamer consisting of 28 receiver offsets between 1 and 7 km. In addition, 28 equally spaced sources from 0 to 12 km were used, and six frequencies logarithmically spaced from 0.05 to 1.6 Hz were generated. To calculate inline electric fields for the salt models, the finite-element-based frequency-domain 2.5-D EM modeling algorithm [24] is used. Fig. 3 shows an example of calculated electric fields according to CMP and offset, which reflect the subsurface spatial resistivity variations well.

The input image of the CNN is generated from electric fields calculated with an EM modeling algorithm (Fig. 4). The horizontal axis and vertical axis of the input image represent the CMP index and the offset index, respectively. The image size is 28 × 28, according to the number of sources and receivers used. In this letter, the image size is equal to the number of sources and receivers we set. If the ranges of CMP and offset are similar to our survey configuration, one can resize the field image with down or upsampling to fit the input size. Thus, even if a data set has missing points due to field conditions, it can be used as the input image with appropriate preprocessing such as interpolation. The input image channel is composed of the frequency used, with real and imaginary components; for this letter, the size is 12, which is the product of 6 and 2. Input images are generated through numerical modeling of 15 200 salt models.

C. Designing and Training Network Architecture

To determine the subsurface electrical resistivity structure from the electric field, we discretize the subsurface into 50 m × 50 m blocks and find the electrical resistivity of each block. To simplify the process, we focus on the center of the salt region, excluding the seawater layer and 3 km on both sides. As a result, the label consists of 11 440 blocks in the range of 0.3 to 2.5 km in the z-direction and 3 to 16 km in the x-direction.

The architecture of the proposed network is tabulated in Table I. This CNN contains four convolutional layers, two maxpooling layers, two fully connected layers, and a loss function connected to the final output. Because the batch

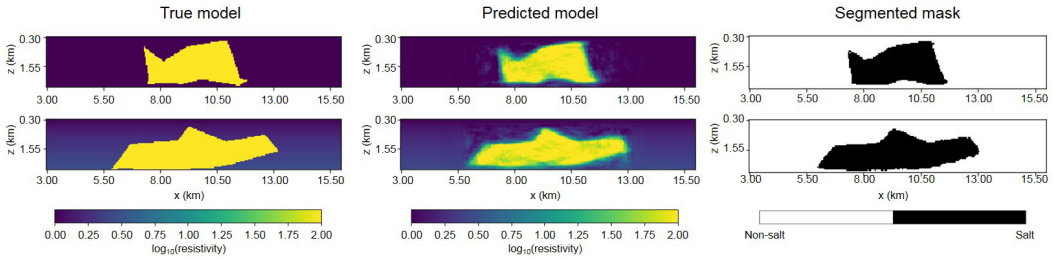

Fig. 5. Examples of prediction results for the validation data set. The left, center, and right columns represent the true electrical resistivity models, predicted electrical resistivity models, and segmented masks separated by salt and nonsalt, respectively.

TABLE I
CNN ARCHITECTURE

Type	Filters	Size/Stride	Input Size	Output Size
Convolutional	64	3×3/1	28×28×12	28×28×64
Convolutional	64	3×3/1	28×28×64	28×28×64
Max-pooling		2×2/2	28×28×64	14×14×64
Convolutional	128	3×3/1	14×14×64	14×14×128
Convolutional	128	3×3/1	14×14×128	14×14×128
Max-pooling		2×2/2	14×14×128	7×7×128
Fully-connected	8192		7×7×128	8192
Fully-connected	8192		8192	11440
Loss function				

TABLE II
PERFORMANCE EVALUATION METRICS FOR VALIDATION DATA SETS

Relative noise (%)	PA	IU		MIU	FWIU
		Salt	Non-salt		
0 (noise-free)	98.61	92.62	98.25	95.44	97.29
1	97.66	87.96	97.09	92.53	95.52
2	95.85	80.33	94.91	87.62	92.41
3	93.83	73.26	92.48	82.87	89.19

normalization reduces the dependence of gradients on the scale of the parameters or their initial values [25], we add a batch normalization layer after each convolutional and fully connected layer. Each batch normalization layer is followed by a leaky rectified linear unit (leaky ReLU) nonlinearity, which has a nonzero gradient over its entire domain [26]. Dropout layers are applied after each leaky ReLU activation to reduce overfitting. The dropout rates are set to 0.1 and 0.2 for convolutional layers and fully connected layers, respectively. The mean-squared error (MSE), the most commonly used regression loss function, is used as the loss function.

During the training phase, a mini-batch gradient descent is applied with sample size 64 to accelerate training. For loss optimization, we use the Adam optimization algorithm [27], which is known for its computational efficiency and excellent performance. The number of training data is determined when the validation loss according to the number of training data shows sufficient convergence. This network is implemented using Google's TensorFlow library [28].

III. EXPERIMENTS

In this section, we predict the subsurface electric resistivity using different input images, including validation and test data containing noise, and evaluate the accuracy of the output results of salt delineation. For the purpose of evaluating performance, we convert the output results of electrical resistivity to a binary mask indicating salt or nonsalt. A threshold resistivity value of 11.22 ($10^{1.05}$) Ωm for binary conversion is selected while training based on the highest intersection over union (IU) of the validation data set. In addition, we use three other common metrics, including pixel accuracy (PA), mean IU (MIU), and frequency-weighted IU (FWIU), for evaluating the segmentation results [29].

A. Prediction Results With Validation Data Set

We first verify the performance of the proposed network using the validation set. Fig. 5 shows examples of the prediction results. The left, center, and right columns of Fig. 5 represent the true electrical resistivity models, predicted electrical resistivity models, and masks, respectively. The electrical resistivity structures predicted through the CNN are very similar to the true electrical resistivity structures. In the predicted electrical resistivity results, the electrical resistivity of the salt boundary is lower than the true electrical resistivity, indicating that the boundary of the salt region in the segmentation result is less reliable than its interior. Quantitative evaluation of the salt delineation of the entire validation data set is shown in Table II. The results for noise-free data show high accuracy in all indicators, especially the salt IU of 92.62%.

During field surveys, noise may be added to the data, which may degrade the prediction results. Therefore, we investigate how sensitive the proposed CNN is to noise despite training with a noise-free data set. In the towed streamer EM survey, noise can be caused by uncertainties in the measurement systems, navigation data, and other factors. The relative noise of the towed streamer EM system mainly depends on the source frequency and offset, and is known to be up to 2% in the frequency and offset range of the source used in this paper [30]. In order to confirm the applicability of the CNN, we use 1%–3% relative noise to consider a more extreme case. Noisy data sets are created by adding normally distributed random noise to the validation data set. Fig. 6 shows the results

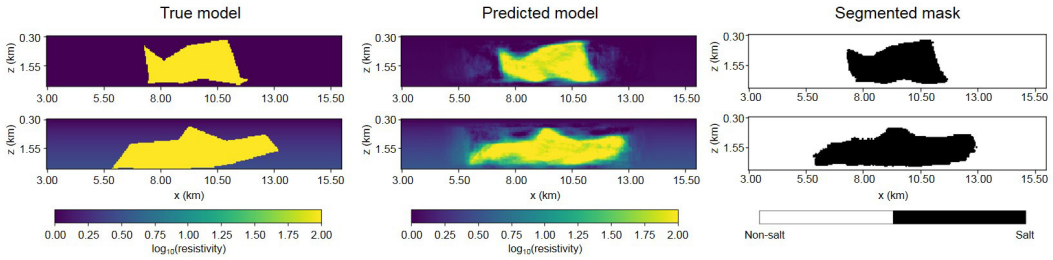

Fig. 6. Examples of prediction results for the 2% noise data set. The left, center, and right columns represent the true electrical resistivity models, predicted electrical resistivity models, and segmented masks separated by salt and nonsalt, respectively.

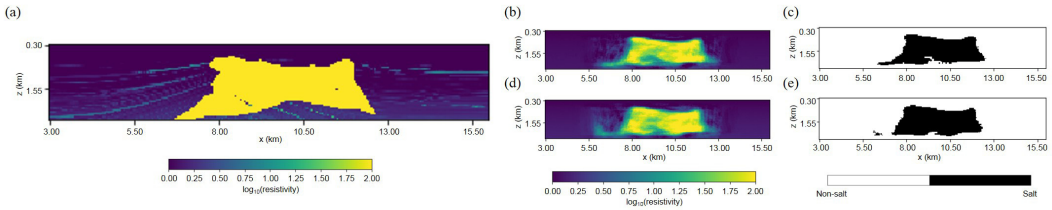

Fig. 7. Prediction results with noise-free and 2% relative noise simulated-SEAM data sets. (a) True electrical resistivity model. (b) and (d) Predicted electrical resistivity models. (c) and (e) Segmented masks separated by salt and nonsalt.

of electrical resistivity prediction with 2% relative noise in the data set. Compared with the case without noise, the region between the electrical resistivity range of the salt and that of the background medium is larger, but the salt region is imaged similarly. In addition, the segmented masks in the right column show that the boundary of the salt region is smoothed due to the noise. Quantitative evaluation results for noisy data sets are presented in Table II. As shown in Table II, the IUs of the salt with up to 2% noise are greater than 80%, which is sufficient for accurate delineation, while that for the extreme case (3% noise) is insufficient, at 73.26%.

B. Application to Simulated-SEAM Data Set

Actual background media may have neither homogeneous nor gradually increasing, but rather complex, electrical resistivity distributions. In addition, there may be hydrocarbon reservoirs adding to the complexity of the background. To consider the complexity of real field data, we use the SEAM 3-D salt model, which was developed as a highly realistic 3-D geological and geophysical model that includes reservoirs with a massive salt body [31], to investigate whether the proposed CNN can distinguish a salt structure against a complex background. In this letter, we use a 2-D horizontal resistivity section at North 20.4 km in the 3-D SEAM model. We call this model the "simulated-SEAM model" and the test data set from this model is designated the "simulated-SEAM data set." As shown in Fig. 7(a), the background medium of the simulated-SEAM model has alternating layered structures with various electrical resistivities and includes reservoirs around the salt body.

Fig. 7(b) and (d) shows the predicted electrical resistivity models for noise-free and 2% relative noise added simulated-SEAM data sets, respectively, and Fig. 7(c) and (e) shows the corresponding salt-segmented masks. First, the result from the noise-free data shows that the salt is reliably imaged, although the background of the simulated-SEAM model is complex, in contrast to the training-phase data. Although electrical resistivity values in the vicinity of the salt are not accurately predicted, the segmented mask with the threshold selected from training clearly indicate the top, sides and even underside of the salt body. Next, the predicted result from the data set with 2% noise shows a slightly distorted electrical resistivity distribution, especially at the sides and bottom of the salt, but the segmented mask still provides an informative salt image. Performance evaluation of the results from simulated-SEAM data sets is shown in Table III. All metrics represent fairly accurate results, especially in the salt IU, which remains over 80% even with 2% relative noise. Thus, we confirmed that the proposed CNN could be applied to data obtained from a complex model of the background medium, such as the simulated-SEAM model.

Another advantage of the proposed method is that it is very efficient for inferring electrical resistivity structures from new data. The inference for a single data set takes only about 0.18 s using a server-grade CPU Intel Xeon E5-2650. In addition, while traditional geophysical inversion can identify the subsurface electrical resistivity structure after sufficient trials by controlling various parameters, such as the initial model and regularization method, the proposed CNN can predict electrical resistivity structures efficiently without expert efforts of a human, as long as the training is well performed.

IV. Discussion

We approached the problem of salt delineation as a regression problem instead of a segmentation problem, which is more appropriate for differentiating salt from other sediments. The reason for this approach is that we think this letter is not only about delineation of salt bodies but rather provides a starting point for obtaining subsurface resistivity distributions using ML with EM data sets. The predicted results for the

TABLE III
PERFORMANCE EVALUATION METRICS FOR SIMULATED-SEAM DATA SETS

Relative noise (%)	PA	IU		MIU	FWIU
		Salt	Non-salt		
0 (noise-free)	95.96	83.03	94.97	89.00	92.35
1	95.91	82.85	94.90	88.88	92.26
2	95.18	80.11	94.02	87.07	90.97
3	93.97	78.08	92.54	84.31	88.93

validation data suggest the possibility of accurate inference of the electrical resistivity distribution of the surrounding media. Even though the results for simulated-SEAM data do not show the exact resistivity distribution of the medium surrounding the salt, this limitation can be overcome by training the CNN with models that include various surrounding media. In addition, to predict the accurate electrical resistivity distribution even in the presence of strong noise, we will conduct a study on the training with noise added data.

V. CONCLUSION

In this letter, we propose a CNN to identify the subsurface electrical resistivity structure from towed streamer EM data. For the purpose of salt identification, salt models of arbitrary shape and size were created, and many input images were generated through numerical EM modeling. The architecture of the CNN was designed to identify the electrical resistivity of each block, thus discretizing the subsurface, and batch normalization and dropout were applied to avoid overfitting and find the optimal solution. The prediction results using validation data sets showed the applicability of CNNs for imaging electrical resistivity from EM data. Moreover, applying the trained CNN to the simulated-SEAM data set, we demonstrated the efficiency and stability of our method, which exhibits remarkable accuracy in salt identification. In addition, the IU of salt was greater than that of 80% despite the presence of noise, indicating that this is a very reliable method. Consequently, segmentation of the predicted electrical resistivity can be used to identify the definite boundary of the salt body, which is difficult to obtain from conventional EM inversion.

REFERENCES

[1] B. Arntsen, C. Gerea, and T. Røsten, "Imaging salt bodies using explicit migration operators offshore norway," *Geophysics*, vol. 74, no. 2, pp. S25–S32, Mar. 2009.

[2] J. P. Leveille, I. F. Jones, Z.-Z. Zhou, B. Wang, and F. Liu, "Subsalt imaging for exploration, production, and development: A review," *Geophysics*, vol. 76, no. 5, pp. WB3–WB20, Sep. 2011.

[3] Z. Jing, Z. Yanqing, C. Zhigang, and L. Jianhua, "Detecting boundary of salt dome in seismic data with edge-detection technique," in *Proc. SEG Tech. Program Expanded Abstr.*, 2007, pp. 1392–1396.

[4] Z. Wang, T. Hegazy, Z. Long, and G. AlRegib, "Noise-robust detection and tracking of salt domes in postmigrated volumes using texture, tensors, and subspace learning," *Geophysics*, vol. 80, no. 6, pp. WD101–WD116, Nov. 2015.

[5] A. A. Aqrawi, T. H. Boe, and S. Barros, "Detecting salt domes using a dip guided 3D Sobel seismic attribute," in *Proc. SEG Tech. Program Expanded Abstr.*, 2011, pp. 1014–1018.

[6] A. Berthelot, A. H. S. Solberg, and L.-J. Gelius, "Texture attributes for detection of salt," *J. Appl. Geophys.*, vol. 88, pp. 52–69, Jan. 2013.

[7] S.-P. Yong, Y. Y. Chen, and C. E. Wan, "Seismic image recognition tool via artificial neural network," in *Proc. IEEE 14th Int. Symp. Comput. Intell. Informat. (CINTI)*, Budapest, Hungary, Nov. 2013, pp. 399–404.

[8] Y. Jia and J. Ma, "What can machine learning do for seismic data processing? An interpolation application," *Geophysics*, vol. 82, no. 3, pp. V163–V177, May 2017.

[9] S. Yuan, J. Liu, S. Wang, T. Wang, and P. Shi, "Seismic waveform classification and first-break picking using convolution neural networks," *IEEE Geosci. Remote Sens. Lett.*, vol. 15, no. 2, pp. 272–276, Feb. 2018.

[10] A. Amin and M. Deriche, "Salt-dome detection using a codebook-based learning model," *IEEE Geosci. Remote Sens. Lett.*, vol. 13, no. 11, pp. 1636–1640, Nov. 2016.

[11] M. Alfarraj, Y. Alaudah, Z. Long, and G. AlRegib, "Multiresolution analysis and learning for computational seismic interpretation," *Lead. Edge*, vol. 37, no. 6, pp. 443–450, Jun. 2018.

[12] A. U. Waldeland, A. C. Jensen, L.-J. Gelius, and A. H. S. Solberg, "Convolutional neural networks for automated seismic interpretation," *Lead. Edge*, vol. 37, no. 7, pp. 529–537, Jul. 2018.

[13] Z. Wang, H. Di, M. A. Shafiq, Y. Alaudah, and G. AlRegib, "Successful leveraging of image processing and machine learning in seismic structural interpretation: A review," *Lead. Edge*, vol. 37, no. 6, pp. 451–461, Jun. 2018.

[14] W. Wang, F. Yang, and J. Ma, "Automatic salt detection with machine learning," in *Proc. 80th EAGE Conf. Exhib.*, 2018, Paper Tu P6 01, doi: 10.3997/2214-4609.201800917.

[15] O. Ronneberger, P. Fischer, and T. Brox. (2015). "U-Net: Convolutional networks for biomedical image segmentation." [Online]. Available: https://arxiv.org/abs/1505.04597

[16] S. Constable and L. J. Srnka, "An introduction to marine controlled-source electromagnetic methods for hydrocarbon exploration," *Geophysics*, vol. 72, no. 2, pp. WA3–WA12, Mar. 2007.

[17] C. Anderson and J. Mattsson, "An integrated approach to marine electromagnetic surveying using a towed streamer and source," *First Break*, vol. 28, no. 5, pp. 71–75, May 2010.

[18] F. L. Engelmark, J. Mattsson, and J. Linfoot, "Marine CSEM with a novel towed acqusition system," in *Proc. PGCE*, 2012, pp. 345–350.

[19] A. Mckay, J. Mattson, and Z. Du, "Towed streamer EM—Reliable recovery of sub-surface resistivity," *First Break*, vol. 33, no. 4, pp. 75–85, Apr. 2015.

[20] D. Yoon, M. S. Zhdanov, J. Mattsson, H. Cai, and A. Gribenko, "A hybrid finite-difference and integral-equation method for modeling and inversion of marine controlled-source electromagnetic data," *Geophysics*, vol. 81, no. 5, pp. E323–E336, Sep. 2016.

[21] M. S. Zhdanov, D. Yoon, and J. Mattsson, "Rapid imaging of towed streamer EM data using the optimal synthetic aperture method," *IEEE Geosci. Remote Sens. Lett.*, vol. 14, no. 2, pp. 262–266, Feb. 2017.

[22] A. Kadu, T. van Leeuwen, and W. A. Mulder, "Salt reconstruction in full-waveform inversion with a parametric level-set method," *IEEE Trans. Comput. Imag.*, vol. 3, no. 2, pp. 305–315, Jun. 2017.

[23] M. S. Zhdanov, M. Endo, D. Yoon, M. Cuma, J. Mattsson, and J. Midgley, "Anisotropic 3D inversion of towed-streamer electromagnetic data: Case study from the troll west oil province," *Interpretation*, vol. 2, no. 3, pp. SH97–SH113, Aug. 2014.

[24] S. Kang, S. J. Seol, and J. Byun, "A feasibility study of CO_2 sequestration monitoring using the mCSEM method at a deep brine aquifer in a shallow sea," *Geophysics*, vol. 77, no. 2, pp. E117–E126, Mar. 2012.

[25] S. Ioffe and C. Szegedy. (2015). "Batch normalization: Accelerating deep network training by reducing internal covariate shift." [Online]. Available: https://arxiv.org/abs/1502.03167

[26] A. L. Maas, A. Y. Hannun, and A. Y. Ng, "Rectifier nonlinearities improve neural network acoustic models," in *Proc. Int. Conf. Mach. Learn.*, vol. 30, no. 1, 2013, p. 3.

[27] D. P. Kingma and J. Ba. (2014). "Adam: A method for stochastic optimization." [Online]. Available: https://arxiv.org/abs/1412.6980

[28] M. Abadi *et al.* (2016). "TensorFlow: Large-scale machine learning on heterogeneous distributed systems." [Online]. Available: https://arxiv.org/abs/1603.04467

[29] J. Long, E. Shelhamer, and T. Darrell, "Fully convolutional networks for semantic segmentation," in *Proc. IEEE Conf. Comput. Vis. Pattern Recognit.*, Jun. 2015, pp. 3431–3440.

[30] J. Mattsson, P. Lindqvist, R. Juhasz, and E. Björnemo, "Noise reduction and error analysis for a towed EM system," in *Proc. SEG Tech. Program Expanded Abstr.*, 2012, pp. 1–5.

[31] M. Fehler and K. Larner, "SEG advanced modeling (SEAM): Phase I first year update," *Lead. Edge*, vol. 27, no. 8, pp. 1006–1007, Aug. 2008.